Effect of Triggering Mechanism on the Load-Displacement Response and Folding Pattern of Square Aluminum Tubes

H. El-Hage[1], P. K. Mallick[2] and N. Zamani[1]
[1]*University of Windsor, Windsor, Ontario, Canada*
[2]*University of Michigan-Dearborn, Dearborn, MI, USA*

Abstract

A systematic numerical investigation of the effect of triggering mechanism on the load-displacement characteristics and lobe formation of square aluminum tubes subjected to quasi-static axial compressive load is presented. Among the physical triggering mechanisms considered were chamfering, drilled holes, geometric imperfection and combinations thereof. The effect of corner radius was also considered. This study has shown that the triggering mechanism controls the load-displacement response as well as the folding pattern. Even though the folding initiation force varies significantly with triggering mechanism, the mean load does not vary greatly. The load-displacement response does not depend appreciably on the corner radius; however, the folding initiation force is lower when a rounded corner is used instead of sharp corners. The folding pattern is also influenced by the corner radius.

Introduction

In axial crushing of thin-walled tubes, a triggering mechanism or a crush initiator is often used to initiate progressive folding of the tube. Experimentally, the triggering mechanism may be as simple as a chamfer machined at the loaded end of the tube or a series of holes drilled on the walls close to the loaded end of the tube. Langseth et al. [1] used geometric imperfection of the shape of a half cosine wave on one of the walls of the tube. The triggering mechanism used in vehicle rails is a series of convolutions or small cut outs located strategically along their length.

In this numerical study, the effect of triggering mechanism on the force-displacement response and folding pattern of a square thin-walled aluminum tube in a quasi-static axial crush test was investigated using LS-DYNA. The triggering mechanism included a chamfer, a series of holes and a geometric imperfection. In addition, the effect of corner radius was also investigated. In some of the numerical models, a combination of triggering mechanisms was considered.

Triggering Mechanisms

Fig. 1 shows the schematic of the thin-walled square aluminum tube considered in this study. The outer dimensions of the tube were 25.4 mm x 25.4 mm, the wall thickness was 1.6 mm and the length was 140 mm. The bottom end of the tube was assumed to be built in and was constrained in all degrees of freedom. The loading plate was assumed to be a rigid plate of 100-kg mass and the loading velocity was 100 mm/sec. The Belytschko-Tsay (BT) shell elements with 5 integration points through the thickness and one integration point in the plane of the shell were used in the numerical models. The element size was 2.5 mm x 2.5 mm. Material 24 was used to model the material's stress –strain behavior.

Twelve different numerical models were created for the triggering mechanism study. They are listed in Table 1. Two of these models (Models 1 and 9) did not have any physical triggering mechanism. The others contained either a single triggering mechanism or a combination of

triggering mechanisms. The tubes in Models 1-8 had sharp corners and the tubes in Models 9-12 had rounded corners of 1.6-mm corner radius. The physical triggering mechanisms are as follows.

- **Chamfering:** In many quasi-static axial crushing experiments [2], an external chamfer is used at the loading end of the tube. For numerical simulations, Matzenmiller and Schweizerhof [3] represented such a chamfer with elements of progressively reduced thickness. A similar approach was used here. The chamfer was represented by a row of elements that were 0.8 mm thick and 2.5 mm in height (Fig. 2). The chamfer angle was 35.5^{o}.

- **Triangular Hole Pattern:** A triangular pattern of holes was used near the loaded end of the tube (Fig. 3). The hole diameter was 3.5 mm. In practice, these holes can be either drilled or punched on all four walls of the tube.

- **Geometric Imperfection:** The geometric imperfection considered here was a variation in mean dimensions of the tube along its length. The mean dimensions of the perfect tube were 23.8 mm x 23.8 mm. The mean dimensions of the tube with geometric imperfections were assumed to be 24 mm x 24 mm for the top 1/3 rd of its length, 23.6 mm x 23.6 mm for the middle 1/3rd of its length, and 23.8 mm x 23.8 mm for the bottom 1/3rd of its length.

Results

For the sake of brevity, only the force-displacement responses and the folding patterns of Models 1-4 are described in details.

Model 1: This model does not contain any physical triggering mechanism. The corners of the cross section were also sharp. Fig. 4 shows the force-displacement response for Model 1 and Fig. 5 shows the corresponding folding pattern. Even though there were no physical triggering mechanisms in this model, the tube walls folded progressively, forming continuous inward and outward thin folds in a symmetric pattern. The folding initiation force observed in the force-displacement diagram was 28,800 N, at which folding was initiated in the tube.   The triggering in this case may have occurred due to lack of numerical precision of the software, hardware or both.

Model 2: This model contained a 35.5^{o}-chamfered end, which was located at the loading end of the tube.   The force-displacement response and the folding pattern for Model 2 are shown in Figs. 4 and 5, respectively.   With the chamfered end, the folding initiation force was 24,600 N, which was significantly lower than that in Model 1. From Fig. 4, it can also be observed that the mean crushing force was lower with the chamfered tube. Before the folding initiation force was reached, there was a smaller peak at which the 0.8 thick mm elements in the chamfered zone started to collapse. After the folding initiation force was reached, the tube walls deformed progressively forming alternating inward and outward thick folds in two connecting edges. This type of deformation is referred to as asymmetric folding mode [4]. The relatively long folding length or the relatively long distance between two consecutive hinges decreased the mean crushing force. The force range in the progressive folding zone was also decreased. It is interesting to note that the folding pattern and the lobe shapes of Model 2 were different from those observed in Model 1. The folding pattern of Model 2 was similar to the folding pattern observed in quasi-static experiments with square tubes containing a chamfered end [2].

Model 3: In Model 3, a triangular pattern of holes was used as the physical triggering mechanism. Unlike Model 1 and Model 2, Model 3 did not exhibit an initial high peak (Fig. 6). In Model 3, folding was initiated by the collapse of the holes at the first folding initiation force, which was observed at 19,900 N. Thus, the folding initiation force in this case was 31 percent lower than that of Model 1 and 19 percent lower than that of Model 2. After folding initiation, the average peak and valley forces of Model 3 were similar to their counterparts of Model 1. The folding pattern of Model 3 was symmetric (Fig. 5), which was similar to that of Model 1.

Model 4: The triggering mechanism in Model 4 was a geometric imperfection. Fig. 7 shows the force-displacement curve of Model 4 and compares it with that of Model 1. The folding initiation force of Model 4 was slightly lower than that of Model 1. The folding in Model 4 started at the geometric imperfection instead of at the loading end. After the folding was initiated, the force decreased gradually and the next force peak occurred at a much larger displacement than that in Model 1. The tube wall deformed progressively forming alternating inward and outward thick folds in two connecting edges, much like in Model 2.

Table 2 summarizes the folding initiation forces, mean crush forces and folding patterns of all twelve models. The folding initiation force and the displacement at folding initiation were very much dependent on the triggering mechanism. The presence of physical triggering mechanism helped reduce the folding initiation force. The lowest folding initiation force was obtained with the triangular hole pattern. In this case, the forces required for progressive folding propagation were close to the folding initiation force.

A comparison of the load-displacement responses of models with sharp corners and rounded corners showed that the general behavior of the load-displacement response did not change appreciably. However, Models 9, 11 and 12 started to fold with symmetric mode of folding as in the case of Models 1, 3 and 8, but, after one or two symmetric fold formation, changed to asymmetric mode. Thus, Models 9, 11 and 12 showed a mixed mode of folding (Fig. 8).   The folding initiation forces for the tubes with rounded corners were also lower than the folding initiation forces for the tubes with sharp corners.

Conclusions

Progressive folding in square aluminum tubes can be triggered using a variety of crush initiators. Physical crush initiators such as chamfers and hole patterns are often used in experiments. This study has shown that minor geometric imperfection in the tube can also initiate progressive folding. This study has also shown that progressive folding in numerical models does not require the presence of a physical triggering mechanism, since lack of numerical precision can also initiate progressive folding.

Both the force-displacement response and the folding pattern are influenced by the triggering mechanism. Depending on the triggering mechanism, two principal types of folding patterns were observed: symmetric and asymmetric. In some cases, a mixed mode of folding containing both symmetric and asymmetric folding patterns was observed

References

1. Langseth, M. Hopperstad, O.S. and Berstad, T., "Crashworthiness of Aluminium Extrusions: Validation of Numerical Simulation, Effect of Mass Ratio and Impact Velocity", International Journal of Impact Engineering, Vol. 22, pp.829-854 (1999).

2. Babbage , J. and Mallick, P. K., "Axial Crush Resistance of Aluminum Composite Hybrid Tubes", Proceedings of 17th Annual Technical Conference of the American Society for Composites, Paper No. 070 (2002).

3. Matzenmiller, A. and Schweizerhof, K., "Crashworthiness Simulations of Composite Structures – A First Step with Explicit Time Integration" Nonlinear Computational Mechanics – State of the Art (ed. P. Wriggers and W. Wagner), Springer-Verlag (1991).

4. Santosa, S.P., Wierzbicki, T., Hanssen, A.G. and Langseth, M. "Experimental and   Numerical Studies of Foam-Filled Sections, International Journal of Impact Engineering, Vol. 24, pp.509-534 (2000).

Table 1: Triggering Mechanisms

Type	Model No.	Corner Radius (mm)	Chamfer (35.5°)	Geometric Imperfection	Holes
Sharp Corners	Model 1	0.0	No	No	No
	Model 2	0.0	Yes	No	No
	Model 3	0.0	No	No	Yes
	Model 4	0.0	No	Yes	No
	Model 5	0.0	Yes	Yes	No
	Model 6	0.0	Yes	No	Yes
	Model 7	0.0	No	Yes	Yes
	Model 8	0.0	Yes	Yes	Yes
Rounded Corners	Model 9	1.6	No	No	No
	Model 10	1.6	Yes	No	No
	Model 11	1.6	No	No	Yes
	Model 12	1.6	Yes	No	Yes

Table 2: Effect of triggering mechanism on axial crush characteristics of a square aluminum tube

Model No.	Corner Radius (mm)	Triggering Mechanism	Folding Initiation Force (N)	Displacement at Folding Initiation (mm)	Mean Crush Force(N)	Folding Pattern
1	0	None	28,800	3.67	16,047	Symmetric
2	0	35.5° Chamfer	24,600	3.93	12,676	Asymmetric
3	0	Hole Pattern	19,900	0.953	15,569	Symmetric
4	0	Geometric Imperfection	27,700	2.28	14,233	Asymmetric
5	0	35.5° Chamfer + Geometric Imperfection	22,900	3.38	13,272	Asymmetric
6	0	35.5° Chamfer + Hole Pattern	17,500	4.03	16,067	Symmetric
7	0	Hole Pattern + Geometric Imperfection	19,700	0.986	15,780	Symmetric
8	0	35.5° Chamfer + Hole Pattern + Geometric Imperfection	14,800	1.08	15,792	Symmetric
9	1.6	None	27,000	2.87	16,914	Mixed
10	1.6	35.5° Chamfer	22,400	3.82	12,075	Asymmetric
11	1.6	Hole Pattern	17,900	0.981	13,905	Mixed
12	1.6	35.5° Chamfer + Hole Pattern	16,500	3.88	13,493	Mixed

t_a= 1.6 mm

140 mm

25.4 mm

25.4 mm
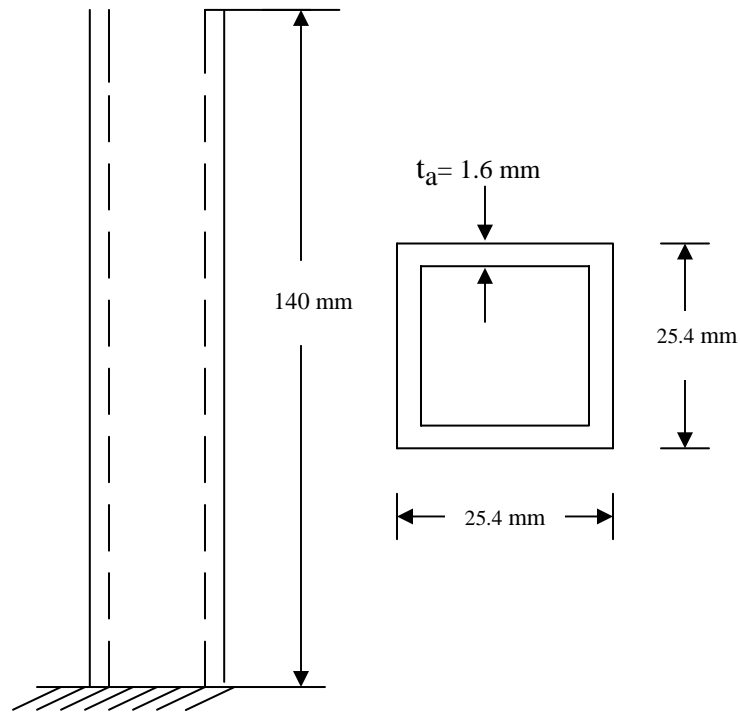
Fig. 1: Schematic of the thin-walled square aluminum tube
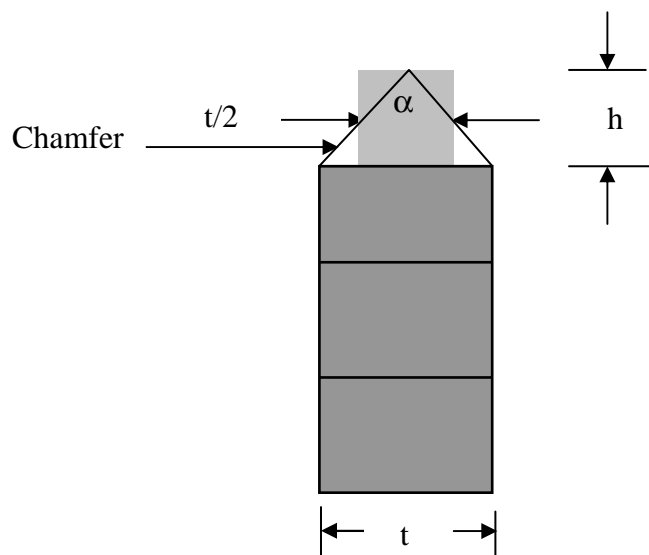
Chamfer

t/2

α

h

t

Fig. 2: Reduced thickness element to represent chamfer at
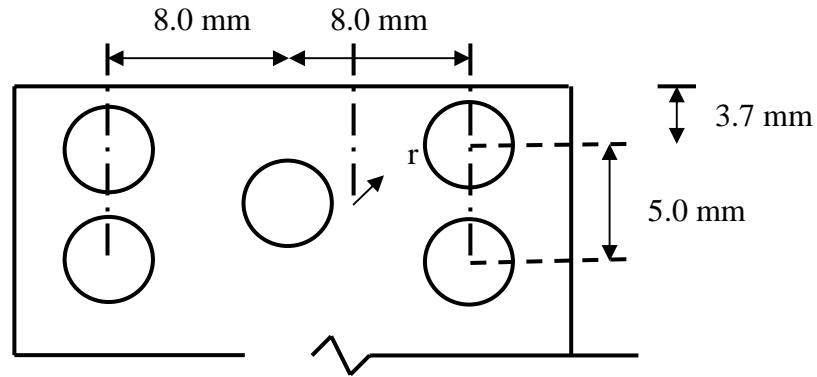the loading end (Chamfer angle = α)

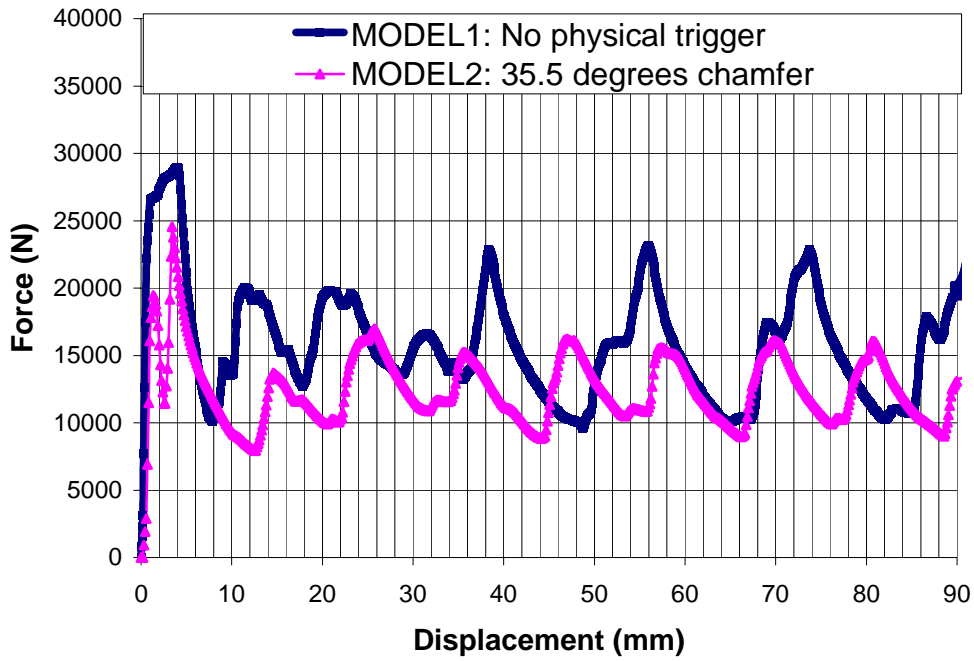**Fig. 3:** Triangular pattern of holes at the loaded end
(r = hole radius = 1.9 mm)

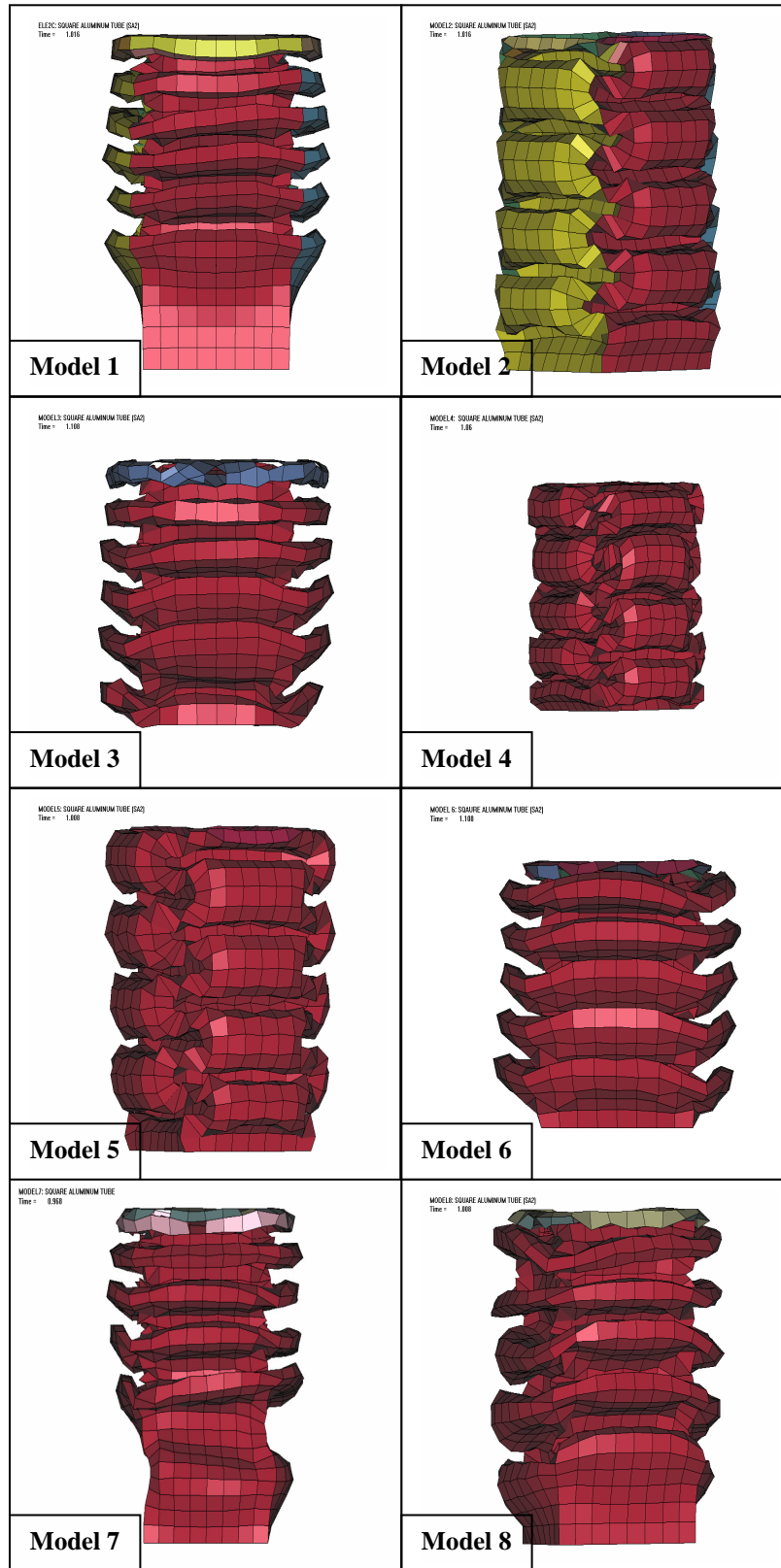**Fig. 4:** Force-displacement responses of Model 1 and Model 2

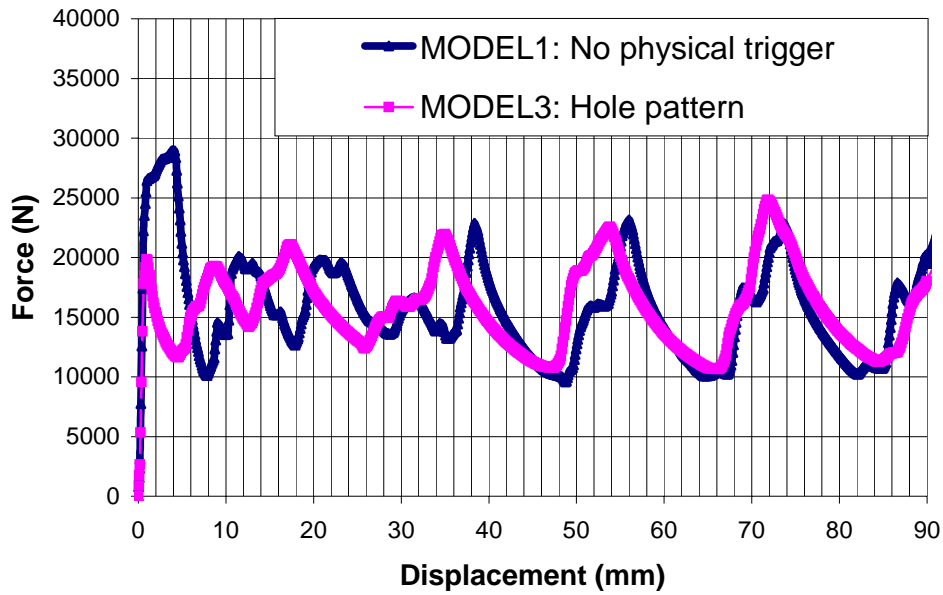**Fig. 5:** Folding patterns of Models 1-8 (tubes with sharp corners)

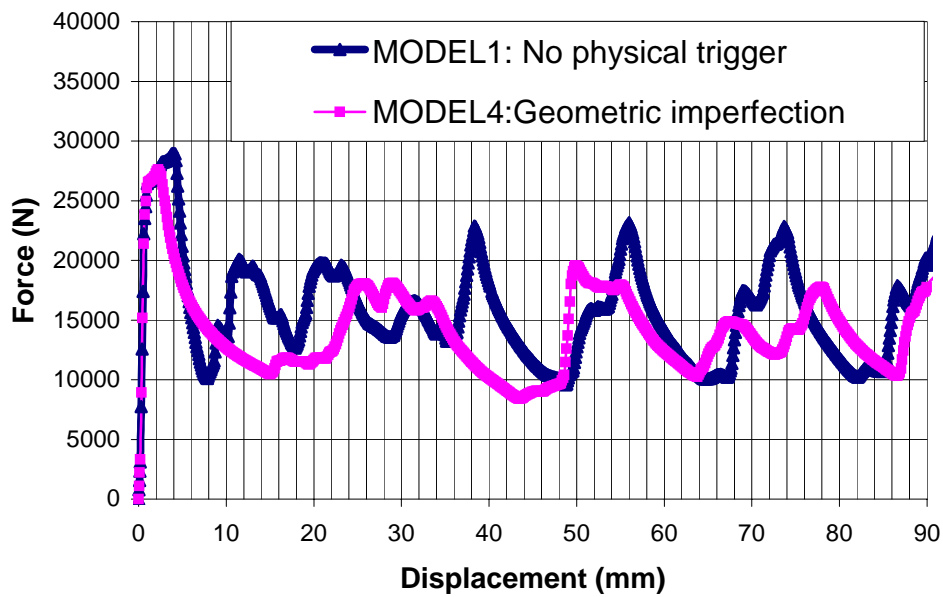**Fig. 6**: Force-displacement responses of Model 1 and Model 3

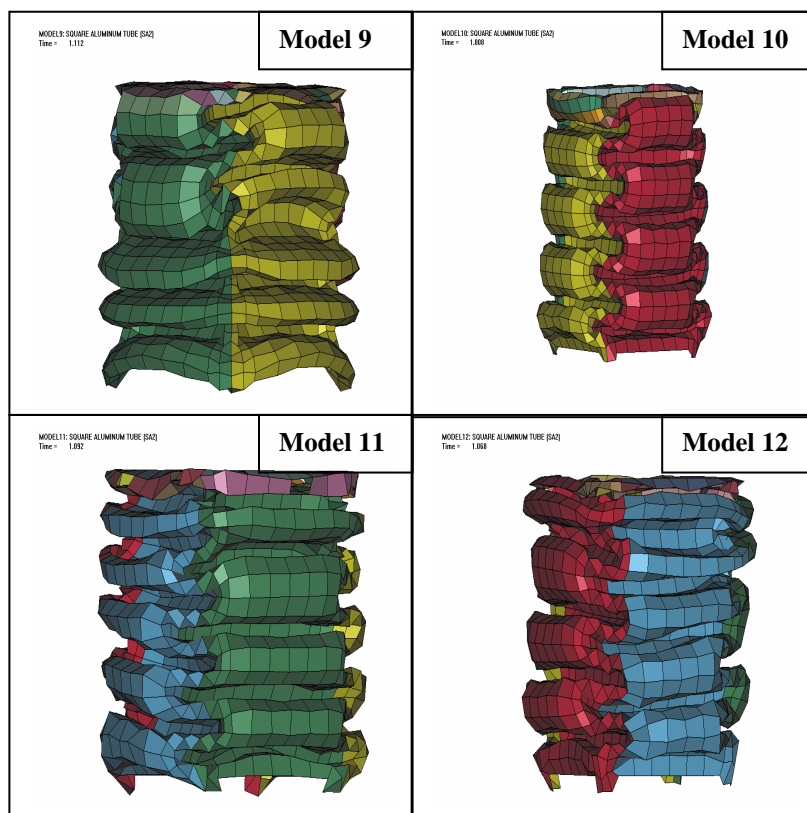**Fig. 7**: Force-displacement responses of Model 1 and Model 4

Fig. 8: Folding patterns of Models 9-12 (tubes with rounded corners)